High, Anisotropic and Substrate-Independent Mobility in Polymer Field-Effect Transistors Based on Pre-Assembled Semiconducting Nanofibrils.

Sara Bonacchi,[†] *Marco Gobbi,*[†] *Laura Ferlauto,*[‡,⊥] *Marc-Antoine Stoeckel,*[†] *Fabiola Liscio,*[‡]

Silvia Milita[‡] *Emanuele Orgiu,*[†§]* *Paolo Samorì*[†]*

[†] University of Strasbourg, CNRS, ISIS UMR 7006, 8 allée Gaspard Monge, F-67000 Strasbourg, France.

[‡] Istituto per la Microelettronica e Microsistemi (IMM) – Consiglio Nazionale delle Ricerche (CNR), Via Gobetti 101, 40129 Bologna, Italy.

Keywords: Organic thin-film transistors, semiconductor-dielectric interface, Langmuir-Schaefer, conjugated polymers, polymer monolayer, film anisotropy.

ABSTRACT

Achieving a nanoscale control over the crystalline structure and morphology of electroactive polymer films as well as the possibility to transfer them onto any solid substrates are important tasks for the fabrication of high-performance organic/polymeric field-effect transistors (FETs). In this work, we demonstrate that ultra-thin active layers pre-assembled at the water/air interface can possess high, anisotropic and substrate-independent mobility in polymer FETs. By exploiting a modified approach to the Langmuir-Schaeffer technique, we self-assemble conjugated polymers in fibrillar structures possessing controlled thickness, nanoscale structure and morphology; these highly-ordered nanofibrils can be transferred unaltered onto any arbitrary substrate. We show that FET based on these films possess high and anisotropic hole mobility approaching 1 $cm^2V^{-1}s^{-1}$ along the nanofibrils, being over one order of magnitude beyond the state-of-the-art for Langmuir-Schaefer polymer FET. Significantly, we demonstrate that the FET performances are independent on the chemical nature and dielectric permittivity of the substrate, overcoming a critical limit in the field of polymer FETs. Our method allows the fabrication of ultra-thin films for low-cost, high-performance, transparent and flexible devices supported on any dielectric substrate.

In the last decade, the performance of polymer field-effect transistors (FETs) have steeply improved, making them a real alternative to amorphous silicon.[1-5] Polymer FETs with p-type and n-type mobility exceeding 10 and 5 $cm^2V^{-1}s^{-1}$, respectively,[6-8] have been demonstrated, being over two orders of magnitude larger than just a decade ago.[9] Such performance improvement was made possible not only through the progress in the molecular design of the semiconducting polymer,[10-12] but also by optimizing the crystalline structure and film morphology of the active layer,[13,14] and by tuning its interfacing with the electrodes[15] and dielectric substrate.[16] In particular, the molecular self-assembly at surfaces to form semiconducting nanostructures to be integrated in working devices depends primarily on the chemical and morphological properties of the chosen substrate and on the processing method employed for the film preparation.

Different processing methods have been so far employed to fabricate high-performance polymer FETs including dip-coating,[17,18] zone-casting,[19] capillarity on pre-engraved substrates[20-22] and bar-coating.[23] All these sophisticated wet-chemistry processing methods provide film morphologies optimized for charge transport, in which uniaxially-aligned polymer chains assemble into highly-ordered parallel nanostructures. Such film structures are highly anisotropic, with charge mobility being higher along the polymer chains direction and lower in the direction perpendicular to them.[17,19,20,23] Although being very intriguing, these techniques are not widely applicable: they are complex and not universal since they frequently require dedicated substrate treatments and are therefore compatible with a limited range of substrates. More generally, the choice of a suitable substrate is a major hurdle in organic electronics because the molecule-substrate interaction is a key parameter governing the self-assembly process during the film formation.[24,25] For example, one of the major drawback of the widely-used strategy for modifying the dielectric/semiconductor interface *via* chemisorbed self-assembled monolayer (SAM), is its

high specificity that prevents the same polymer from forming similar structure when adsorbed on different SAMs.[26] Likewise, the possibility of obtaining the same supramolecularly engineered organic thin-film onto any arbitrarily solid support is of notable importance because the dielectric permittivity of the substrates when it is employed as gate dielectric, strongly effects the charge carrier mobility of the OFET.[27-30] Moreover, *ad hoc* orthogonal solvents are required to spin-coat semiconducting polymer onto organic substrates.[31]

In this work, we demonstrate high, anisotropic and substrate-independent hole mobility in polymer films obtained by a modified approach to the Langmuir-Schaeffer (LS) technique.[32,33] Our facile, efficient and generally-applicable strategy allows us to pre-assemble polymer films at the water-air interface, and transfer them easily onto very different substrates, overcoming the need of orthogonal solvents. In particular, we go beyond standard LS method, by exploiting its potential not only to form a monolayer but also to generate thicker high-performing films with active control over their nanostructure and morphology. By tuning two simple experimental parameters such as the volume of the polymer solution spread onto the water and the surface pressure selected to transfer the film onto the solid substrate, we demonstrate the ability to obtain ultra-thin layers (at the monolayer limit) or thicker (2-to-3 layers) and denser films. A combined optical and micro-structural analysis of the transferred films provides evidence that the films are characterized by long-range well-ordered nanofibrils, resulting in a highly-anisotropic structure, independently on the nature of the substrate. While FETs based on polymer monolayers possess rather poor electrical performances (hole mobility $\mu \approx 0.04$ $cm^2V^{-1}s^{-1}$), those based on thicker films possess a remarkably-high anisotropic hole mobility approaching 1 $cm^2V^{-1}s^{-1}$along the nanofibrils. The latter value represents a record for Langmuir-Schaefer polymer FETs, being almost two orders of magnitude beyond the state-of-the-art,[34-37] thus highlighting the importance

of our modified approach to the LS technique. Moreover, we have fabricated FETs based on polymer films transferred on three different organic dielectric substrates without using specific orthogonal solvents. Interestingly, we demonstrate that the FET performances are independent on the chemical nature of the dielectric substrate and of its dielectric permittivity, since the assembly of the active layer is pre-determined at the water/air interface. In perspective, our approach enables the fabrication of multi-layered heterostructures composed by layers of different polymers, resulting in an artificial multicomponent materials featuring unconventional properties.

RESULTS AND DISCUSSION

Langmuir-Schaeffer is a technique to form molecular monolayers. In its standard use, a diluted solution is spread onto the water surface, forming an expanded phase possessing a low areal density. The movement of the barriers compresses the material to form a monolayer characterized by higher areal density, which is transferred onto the target substrate (Figure 1a).[32] Herein, we adopt a different strategy by starting from a higher amount of material spread on the water surface, forming an already-condensed phase before compression (Figure 1b). The barrier movement is used to increase the thickness and the density of the polymer film, conferring it a structural anisotropy by forcing the polymers to self-assemble into parallel nanofibrils (Figure 1b).

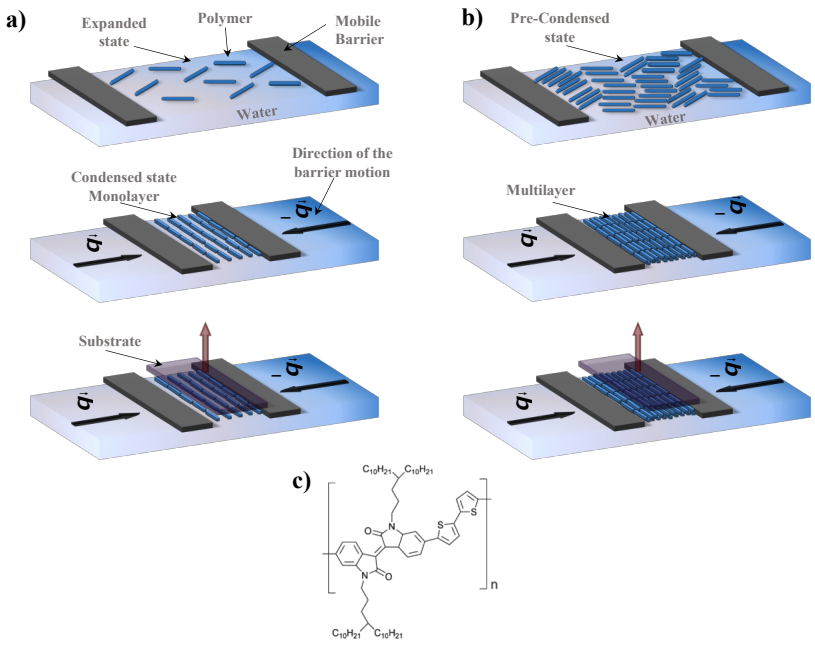

Figure 1. (a) Schematic illustration of the standard Langmuir–Schaefer (LS) transfer process. (b) Schematic illustration of our Langmuir–Schaefer (LS) strategy. (c) Chemical structure of **IIDDT-C3** polymer.

Among the high performing semiconducting polymers available, we have focused our attention on an isoindigo-based conjugated polymer (**IIDDT-C3**) characterized by a branched alkyl chain substituent (Figure 1c).[38] In particular, Lei *et al*. have recently reported that such polymer shows high hole mobility upon high temperature annealing, which deeply modifies the polymer structure.[39,40] In particular, the presence of symmetric branched alkyl side chains makes **IIDDT-C3** polymer an ideal candidate for forming a highly ordered assembly at water/air interface.[34] Moreover, the already reported long-time ambient stability[39] guarantees minor performance degradation due to possible water residuals.

In order to assess whether **IIDDT-C3** is a suitable candidate to form transferable self-assembled layers with our strategy, we prepared films by varying (i) the volume of **IIDDT-C3**

solution (solvent: chloroform; concentration: 0.5 mg/mL) spread over the water sub-phase, and (ii) the surface pressure. In particular, we have focused our attention on three films obtained in different conditions, which will be called hereafter **LS1**, **LS2**, **LS3**. For **LS1** the isotherm curves show a gradual transition from an expanded to a condensed state, indicating the presence of a monolayer film with an edge-on molecular packing at the air/water interface (see Supporting Information), as already reported for polymer films obtained by the standard LS technique.[34] Instead, to form **LS2** and **LS3** we have spread a greater amount of materials on the water surface. For this reason, the isotherm curves for **LS2** and **LS3** do not show any initial expanded phase, suggesting the formation of a condensed film at the air/water interface even prior to compression. Yet, **LS2** possesses a lower areal density compared to **LS3**. All the as-obtained films assembled at the water-air interface were transferred onto a substrate kept parallel to such interface and moved vertically until reaching the polymer beneath (Figure 1b). The transfer is performed at ambient conditions and, remarkably, only a mild thermal annealing at 40 ˚C for 6h is used before the electrical characterization to guarantee full evaporation of residual solvent and water. Further details on the three different types of films are provided in Figure S1 in the Supporting Information.

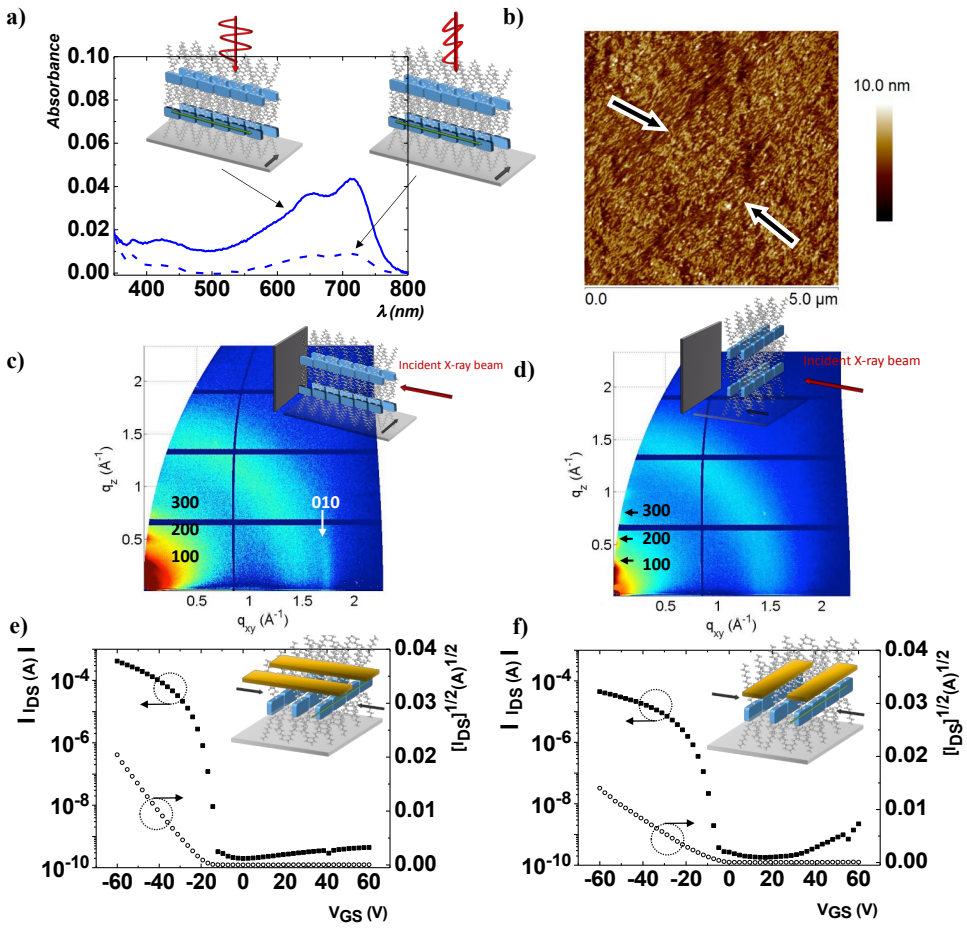

Figure 2. (a) Linearly-polarized light absorption spectra of **IIDDT-C3 LS2** film with the polarization oriented parallel (continuous line) or perpendicular (dashed line) to the direction of the LS barrier closure. (b) Atomic Force Microscopy topography image of **LS2** thin film on a HMDS-treated SiO_2 substrate. Black arrows indicate the direction of the barrier motion. (c, d) 2D-GIXRD patterns of **LS2** film deposited by LS on a HMDS-SiO_2 substrate recorded with the X-ray beam (c) parallel or (d) perpendicular to the average orientation of the nanofibrils. (e, f) Transfer curve recorded on the **LS2** film serving as the active layer in a three-terminal device with carrier transport (e) parallel or (f) perpendicular to the orientation of the polymer nanofibrils.

In order to attain a full characterization of the transferred films, we have studied their optical, morphological, structural and electrical properties. The results of this multi-techniques characterization is displayed in Figure 2 for **LS2**. Figure 2a portrays the linearly-polarized light absorption spectra of **IIDDT-C3** LS films. It reveals a macroscopic optical anisotropy that is not observed in spin-coated films obtained from the same solutions (Figure S3, Supporting Information). In particular, when the incident light is linearly polarized along the direction of the barrier motion (named $\vec{b}$ in Figure 1), the absorption band of the LS film is less intense and less structured than when the polarization is perpendicular to it (absorbance ratio being approximately 4.5). This optical anisotropy can be explained by the presence of one-dimensional supramolecular nanostructures, highly oriented perpendicularly to the barrier motion, as already observed in aligned fibrils obtained by other solution processing methods.[41-44]

The Atomic Force Microscope (AFM) topography images recorded in intermittent contact mode further confirm that LS films are highly anisotropic. In particular, Figure 2b exhibits polymer nanofibrils aligned along the direction perpendicular to $\vec{b}$ (black arrows) with a measured width of ca. 30 nm and length exceeding 1 μm (Figure S4, Supporting Information), being in stark contrast to the random orientation of the polymer aggregates in spin-coated films (Figure S3 and S4, Supporting Information). These features suggest that the compression exerted by the barriers is responsible for the formation of the uniaxially aligned polymer nanofibrils starting from a pristine otherwise-disordered film.[45] Detailed insight into the polymer assembly inside fibrils was obtained by Grazing Incidence X-Ray Diffraction (2D-GIXRD) measurements recorded with the incident X-ray beam aligned either perpendicular (Figure 2c) or parallel (Figure 2d) to $\vec{b}$ (*i.e.* parallel or perpendicular to the nanofibrils direction). Along the q_z direction, several (h00) reflections related to the lamella stacking are observed regardless of the

X-ray beam orientation (Figure 2c,d and Figure S5c in the Supporting Information). On the other hand, on the surface plane direction, a rod (q_{xy} = 1.74 Å^{-1}) ascribed to the π-π stacking between adjacent backbones is observed only when the X-ray beam is oriented parallel to the fibrils orientation (Figure 2c and Figure S5d in the Supporting Information). These results indicate that (i) **IIDDT-C3** lamella tend to organize according to an edge-on configuration with lamella stacking of 2.5 nm and π-π distance of 3.6 Å, and (ii) the LS technique forces the formation of nanofibrils inside which the π-π stacking lies preferentially in the direction perpendicular to the fibrils' long axes. Similar measurements carried out on spin-coated films revealed a marked isotropic features and amorphous structure (Figures S6a, S12b and S13a in the Supporting Information).

The electrical performances of **LS2** films were characterized by integrating such films as active layer in bottom-gate top-contact FETs fabricated by using hexamethyldisilazane (HMDS)-treated SiO_2 substrates. In order to explore the charge transport anisotropy, the source and drain Au contacts were deposited on top of the same LS film, in the direction either parallel or perpendicular to the main axis of the **IIDDT-C3** nanofibrils. The comparison of Figure 2e and 2f provides unambiguous evidence that the hole field-effect mobility is higher when measured along the direction parallel to the main axis of the nanofibril and it amounts to $\mu = 0.25$ cm^{2}V^{-1}s^{-1} (0.08 cm^{2}V^{-1}s^{-1}). Isotropic transport was instead observed for spin-coated FETs which exhibited hole mobility amounting to $\mu = 0.025$ cm^{2}V^{-1}s^{-1} (Figure S7, Supporting Information). Such mobility dependence from the fibrils' orientation in the LS film is in excellent agreement with the results of the structural, morphological and optical characterizations. It is therefore fully consistent with an alignment of the **IIDDT-C3** backbone along the nanofibrils which is favorable for charge transport.[14] Moreover, the hysteresis recorded on the transfer curves of LS-based

transistors was found to be negligible when compared to that of devices prepared by spin-coating (Figure S8 in the Supporting Information). This finding can be attributed to the higher degree of crystallinity which contains less structural defects acting as trapping centers.

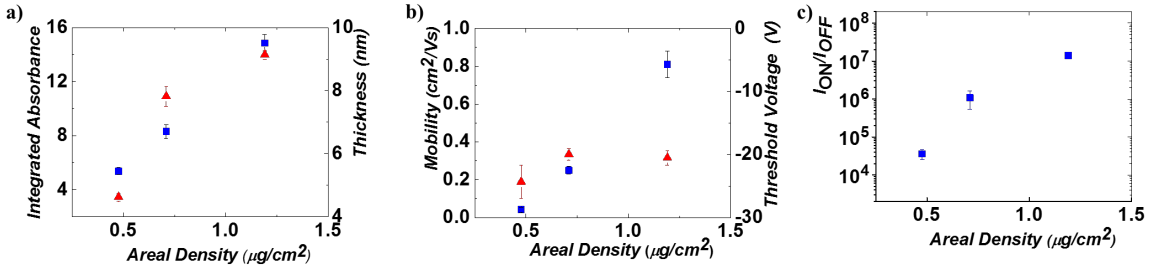

Figure 3. (a) Integrated absorption spectra (blue square) and thickness (red triangle). (b) Hole mobility (blue square) and threshold voltage (red triangle) in saturation regime. (c) I_{ON}/I_{OFF} of LS films of **IIDDT-C3** as a function of the areal density ϱ [V_{DS} = -40 V; L = 80 μm; W = 10 mm; $C_{i[SiO2]} = 1.5\times10^{-8}$ F cm^{-2}]

Figure 3 displays a comparative analysis of the dependence of relevant optical and electrical parameters on the areal density within the formed LS films. Such results were gathered on samples/devices **LS1**, **LS2** and **LS3**, by performing a thorough characterization analogous to the one presented above for **LS2**. On the basis of the volume of solution spread over the water surface and the barrier position at the target pressure, we have estimated the areal density ϱ (expressed in μg/cm^2) for each transferred film, which results in ϱ_1 = 0.48 μg/cm^2, ϱ_2 = 0.71 μg/cm^2 and ϱ_3 = 1.19 μg/cm^2 for **LS1**, **LS2** and **LS3** respectively (Figure S1 in the Supporting Information). The modulation of the areal density ϱ during the LS film growth allows to tune various physical properties of the film and, on the same time, to explain the correlation between the **IIDDT-C3** assembly and the device performances. Morphological and structural characterizations reveal that all the LS films are characterized by aligned nanofibril bundles, similarly to those displayed in Figure 2 for the **LS2** film (AFM images in Figure S3 in the

Supporting Information); moreover, XRD patterns confirm an edge-on packing within all the LS films (Figure S6 in the Supporting Information). We highlight that these data confirm that only **LS1** is a monolayer thick film, since its thickness (4.6 nm) is compatible with the one expected for the edge-on configuration of the polymer. Conversely, the thickness of **LS2** and **LS3** is in the range of two-to-three monolayers. Figure 3a displays the dependence of the integrated intensity of the absorption spectra and of the thickness of the different LS films on the areal density (ϱ). Interestingly, the absorbance increases linearly with ϱ, and in particular **LS3** absorbs three times more than **LS1**, indicating that the quantity of polymer on the substrate in **LS3** is three times greater than in **LS1**. Instead, the thickness of the **LS3** film is only twice that of **LS1** highlighting that **LS3** film is not only thicker but also denser. This higher density implies a tighter inter-fibril packing, as evidenced in the AFM images in Figure S3 and Table S1 in the Supporting Information.

The different film density strongly influences the electrical performances of the devices. Figure 3b shows the dependence of field-effect mobility of LS films on the areal density ϱ (with carrier transport parallel to polymer nanofibril bundles orientation). A strong correlation between the density of the polymer films and the mobility within such films is observed. In particular, the performance of the devices based on LS films increase almost linearly with increasing ϱ from an average mobility of 0.025 $cm^2V^{-1}s^{-1}$and I_{ON}/I_{OFF} of 3.6 x 10^4 for **LS1**, up to 0.9 $cm^2V^{-1}s^{-1}$and I_{ON}/I_{OFF} of 1.4 x 10^7 for **LS3**. The improved I_{ON}/I_{OFF} can be explained by the higher current flowing in ON state for **LS3**. Instead, the mobility enhancement can be attributed to the tighter inter-fibrils packing and thus to the lower defective nature of the films, in excellent accordance with AFM results (Figure S3 in the Supporting Information). In addition, the transition from monolayer **LS1** towards more 3D systems (**LS2** and **LS3**) determines a charge transport scenario

where the carriers can additionally hop along the Z-axis, offering more percolation pathways around structural and electronic defects within the films, which results in a higher field-effect mobility. The threshold voltage exhibits negligible variations with ϱ and it tends to be higher in **LS1** film where some voids, imaged by AFM, could possibly act as source of charge trapping. Remarkably, a maximum mobility as high as 2.7 $cm^2V^{-1}s^{-1}$ and an I_{ON}/I_{OFF} up to 2.5 x 10^8 was measured on **LS3** devices (Figure S10, Supporting Information).

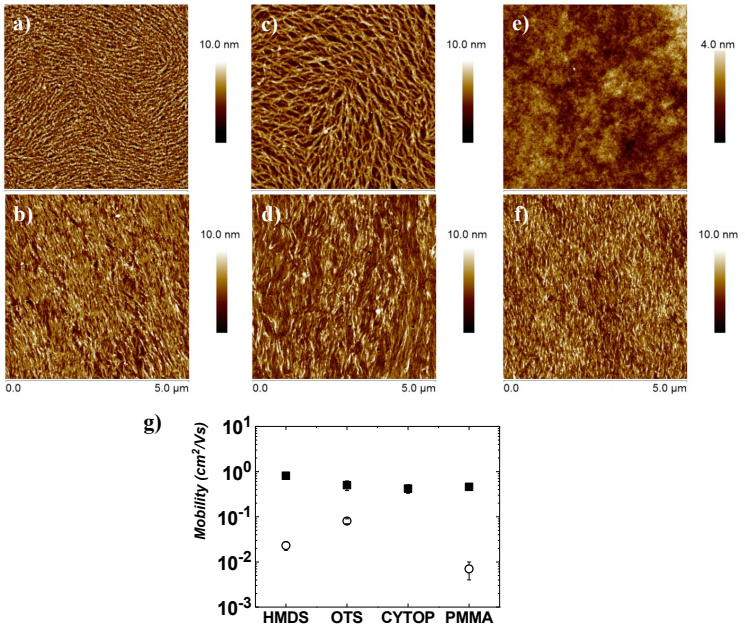

Figure 4. Atomic force microscopy images of (a, c, e) spin-coated **IIDDT-C3** films and, (b, d, f) LS films on different substrates. In particular, (a, b) OTS-treated SiO_2, (c,d) SiO_2 covered with a PMMA layer, and (e,f) SiO_2 covered with a CYTOP layer. (g) Comparative mobility plot of **IIDDT-C3** based devices with either spin-coated (white circle) or LS (black square) films deposited on different substrates.

In order to cast light onto the influence of the substrate type on our films, we have transferred the LS films onto dielectric substrates exposing different chemical groups as well as possessing different wettability and dielectric permittivity (Table S2, Supporting Information). AFM

imaging of the **IIDDT-C3** LS films transferred onto octadecyltrichlorosilane (OTS), poly(methyl methacrylate)(PMMA), CYTOP and UV-Ozone -treated SiO_2 substrates confirm the presence of the typical highly oriented polymer nanofibrils perpendicularly aligned to $\vec{b}$ (Figure 4b,d,f) as reported above for the HMDS-treated SiO_2 substrate. Importantly, the thin-film deposited by spin-coating on the same substrates clearly shows a markedly different morphology, which is characterized by isotropic structures of polymer aggregates randomly oriented. In particular, when the highly hydrophobic CYTOP substrate is employed no trace of the spin-coated **IIDDT-C3** polymer could be imaged by AFM, confirming the versatility limits of this deposition method (Figure 4e). Regardless the nature of the substrates, 2D-GIXRD images of LS films exhibit lamellar peaks along the out-of-plane direction and π-π stacking peak along the in-plane direction when the incident beam is parallel to the nanofibril long axis direction (Figure S13-16, Supporting Information). These findings confirm the independence of the **IIDDT-C3** supramolecular structure on the nature of the substrate, and importantly it confirms the presence of the structural anisotropy within the LS polymer film in all the different samples. Conversely, 2D-GIXRD images collected for spin-coated films do not show any Bragg reflections coming from the films, confirming their amorphous nature as identified from XRR analysis (Figure S12 in the Supporting Information). The electrical properties of these LS films were compared with those prepared with spin-coating on the same substrates (see, Figure S17-19 in the Supporting Information). Interestingly, electron transport seems to be enhanced in LS *versus* SC films. While its investigation is beyond the scope of this work, it will be the object of future work. In all cases, hole mobility was found to be higher in LS films compared to spin-coated ones; in the latter one a highest field-effect mobility of 0.03 $cm^2V^{-1}s^{-1}$ on OTS-treated substrates was measured. An extreme case is when a CYTOP substrate is employed because no source-drain

current was measured in spin-coated films confirming the absence of a continuous **IIDDT-C3** film on top of the dielectric layer. On the contrary, mobility is nearly unchanged in devices prepared by LS deposition regardless of substrate used (Figure 4g and Figure S20 in the Supporting Information). In particular, while charge transport in organic semiconductors strongly depends on dielectric permittivity,[27-29] the devices based on LS polymer were found to feature charge carrier mobilities that would not vary sensibly with ε ranging between 2.1 and 3.9. The latter interval includes a large variety of dielectrics commonly used for organic electronics, therefore our findings represent a substantial progress in such field. Such result can be ascribed to the particular technique and polymer type employed in our study. In particular, (i) the polymer layer is always organized at the water-air interface in an edge-on configuration and its assembly is not influenced by the chemical nature of the substrate over which such layer is deposited afterwards, and (ii) the organic core through which the charge transport takes place is separated by the substrate by long alkyl chains, the latter screening the extrinsic energetic disorder introduced by the dielectric surface.[46] Hence, our approach enables not only to control the film formation but also to guarantee a stronger uniformity of morphology and of transport properties that are not affected by the surface and dielectric properties of the gate insulating layer.

CONCLUSIONS

In conclusion, we have demonstrated that our modified Langmuir-Schaeffer LS deposition is a versatile method which makes it possible to self-assemble π-conjugated polymers into highly ordered thin-films made of tightly packed nanofibrils. When integrated as active layer in OFETs, these semiconducting polymer films exhibited record mobility for LS-film OFETs without the need of any high-temperature annealing. Moreover, we have proved that the electrical

performances are independent both on the chemical nature of the substrate and on the dielectric permittivity of the gate insulator. Importantly, our approach to LS technique potentially enables the formation of large area films (up to 9 cm^2) by using a tiny amount of polymer (~ 75 μg) spread onto the water surface to create high-performance, transparent and flexible devices at low cost regardless of the chemical and dielectric nature of the substrate. In perspective, the possibility to apply this film preparation method to other kinds of conjugated polymers will allow controlled fabrication of multilayered hybrid films without sacrificing morphological and electrical properties of each single layer.

MATERIALS AND METHODS

General: The **IIDDT-C3** (Mw=58,000 Da; polydispersity, PDI = 2.4) polymer was supplied by 1-MATERIAL INC and it was used as received. For all the LS and SC films, a 0.5 mg/mL chloroform solution of **IIDDT-C3** polymer was used. The polarized UV-Vis spectra were recorded at room temperature on a Shimadzu UV3101 spectrometer equipped with Melles Griot polarizer. AFM Characterizations were carried out with a Multimode V (Veeco) microscope equipped with a Nanoscope V controller. Commercial silicon cantilevers with a nominal spring constant of 40 N m^{-1} were used for morphological characterization in intermittent contact mode. Water contact angles (Table SI-2, Supporting Information) were measured by the sessile drop method on a DSA 100 goniometer (Krüss GmbH); milli-Q water was used and data evaluation was done using the software Drop Shape Analysis. The thickness of PMMA and Cytop spin-coated films was evaluated by using an Alpha-Step IQ Surface Profiler (KLA-Tencor).

2D-GIXRD diffraction patterns were collected using the 2D Pilatus detector at the XRD1 beamline of ELETTRA synchrotron facility in Trieste (Italy). The X-ray beam was characterized

by an energy of 12.5 keV (corresponding to λ = 1 Å) and a beam size of 200x200 μm^2. The grazing incident angle was fixed at $\alpha_i = 0.18°$ to maximize the diffraction signal coming from the semiconducting layer at the top of the substrate.

XRR and XRD measurements were carried out with a SmartLab Rigaku diffractometer equipped with a rotating copper anode (λ_{Cu} = 1.54184 Å) followed by a parabolic mirror to collimate the incident parallel beam and a series of variable slits placed before and after the sample to control the beam size and detector acceptance respectively. The beam resolution was 0.01deg and 0.1deg for the out-of-plane and in-plane measurements, respectively.

Substrate Cleaning and Preparation: For optical measurements, TED PELLA quartz slide (1x1 in, 1 mm thick) were used. For all devices, SiO_2/Si-n^{++} substrates (230 ± 10 nm thick SiO_2, 675 ± 20 μm thick Si-n^{++}, Fraunhofer Institute for Photonic Microsystems IPMS, Dresden, Germany) were used. All the substrates were sonicated for 10 min each in acetone and isopropyl alcohol, and dried with nitrogen. For the preparation of OTS-, HMDS- and Cytop- substrates the following procedures were used: the SiO_2/Si-n^{++} substrates were cleaned with UV-Ozone treatment for 5 min prior to use and all the substrates were prepared in glove box under nitrogen atmosphere. For the preparation of OTS- treated silicon dioxide substrate, the SiO_2/Si-n^{++} substrates were immersed in a 5 mM solution of OTS (Aldrich 104817) in toluene inside a sealed jar, then heated at 60˚C for 60 min, exposed overnight to this environment and finally, rinsed in pure toluene bath. For the preparation of HMDS-treated silicon dioxide substrate, HDMS solution (Aldrich 440191) was spin-coated (1500 rpm, 60 sec) onto the substrate and then annealed at 100˚C for 60 min. PMMA (Mw = 120 kDa, Aldrich 182230) was dissolved in hot anhydrous n-butyl acetate (70 mg/mL) and filtered with 0.45 μm PTFE syringe before spin-

coating (1000 rpm, 30 sec) onto SiO_2/Si-n^{++} substrates. The samples were then annealed at 150°C for 120 min (PMMA thickness ~380 nm). Cytop CTL 809M diluted in CT-SOLV180 (190 µl/10 µL respectively) was spin-coated (2000 rpm, 30 sec) onto the SiO_2/Si-n^{++} substrates and then annealed at 150°C for 120 sec (Cytop thickness~735 nm).

IIDDT-C3 polymer film fabrication: Langmuir–Schaefer experiments were carried out in a KSV minitrough apparatus by employing ultrapure MilliQ water with a resistivity of 18 MΩ cm as a subphase. Drops of the **IIDDT-C3** solution (0.5 mg/mL in chloroform) were randomly spread over the aqueous sub-phase with a Hamilton microsyringe. After few minutes to evaporate the solvent, the floating films were linearly compressed by the two mobile barriers at a rate of 5 mm/min. Surface-pressure *versus* molecular-area isotherms were recorded by film balance measurement (Wilhelmy plate method). The ultrathin film transfers were performed onto the different substrates by a horizontal deposition; a different surface pressure was used in function of the spread volume (*i.e.*, 25 mN/m for 50 µL, 35 mN/m for 100 µL and 45 mN/m for 150 µL). Taking into the account the volume of polymer solution spread at the water/air interface and the area between the barriers during the transfer, we estimated the areal density *i.e.*, quantity of polymer for unit area in the different cases (expressed in µg/cm^2). The films were dried in vacuum oven at 40 °C and stored in nitrogen atmosphere before characterization. Spin-coated (SC) films having thickness of ~ 3 nm were fabricated at speed of 3000 rpm for 60 s, from 150 µL of a solution 0.5 mg/mL in chloroform.

Device Fabrication and Characterization: Bottom-gate, top-contact long channels (channel lengths L = 60–120 µm, W = 10 mm) transistors were fabricated on SiO_2/Si-n^{++} on which 35 nm thick interdigitated gold electrodes were thermally evaporated through a shadow mask. A

Keithley 2636A source meter interfaced by LabTracer™ software was employed for the OFETs characterization in the controlled atmosphere of a glovebox (O_2 and H_2O content below 10 and 2 ppm, respectively). The field effect mobility were obtained in the saturation region of transistor operation by using the equation $I_{DS} = \left(W/2L\right) C_i \mu (V_{GS} - V_{th})^2$ where W/L is the channel width/length, C_i is the gate dielectric layer capacitance per unit area, and V_{GS} and V_{th} are the gate and threshold voltages. The dielectric capacitance was determined by using $C_i = \varepsilon_o \varepsilon_r \frac{A}{d}$ where ε_o is the dielectric constant in vacuum, ε_r is the dielectric constant of the material, A is the capacitor area and d is the thickness. The field effect mobilities reported in this paper were measured in devices with channel length, L = 80 μm. In particular, we prepared at least 3 films for each kind of LS films and the average mobility was measured in 2 devices for each film without considering in the statistic the maximum mobility of 2.7 [$cm^2V^{-1}s^{-1}$] obtained for **LS3** (see the Table S3 in the Supporting Information for more details on the statistics of OFET measurements).

ASSOCIATED CONTENT

Supporting Information is available free of charge *via* the Internet at http://pubs.acs.org.

AUTHOR INFORMATION

Corresponding Author

*Address correspondence to samori@unistra.fr , emanuele.orgiu@emt.inrs.ca

Present Addresses

[§]Present address: Institut National de la Recherche Scientifique (INRS), EMT Center, 1650 Boul. Lionel Boulet, J3X1S2 Varennes, CA.

[⊥]Present address: Center for Neuroprosthetics, Interfaculty Institute of Bioengineering, School of Engineering, École Polytechnique Fédérale de Lausanne, Lausanne, Switzerland.

Author Contributions

The experiment was conceived by S.B., M.G. E.O. and P.S.. S.B. and M.-A.S. performed the LS film preparation and the FETs study. L.F., F.L. and S.M. performed the X-Ray characterization. E.O. and P.S. supervised the entire study. S.B and M.G. wrote the manuscript with comments and suggestions from all co-authors.

ACKNOWLEDGMENTS

This work was supported by the EC through the Marie Curie IEF GALACTIC (PIEF-GA-2013-628563), the FET project UPGRADE (GA-309056), the ERC project SUPRAFUNCTION (GA-257305), the Marie Sklodowska-Curie ITN project iSwitch (GA-642196), the Agence Nationale de la Recherche through the LabEx project Chemistry of Complex Systems (ANR-10-LABX-0026_CSC), the International Center for Frontier Research in Chemistry, and the Italian National Project N-CHEM - Flagship NANOMAX. S.B. acknowledges Thibault Chervy (Nanostructures Laboratory, I.S.I.S.) for helping with the linearly-polarized light absorption spectra. L.F. and F.L. thank L. Barba and N. Demitri for optimizing the experimental setup at the XRD1-ELETTRA beamline.

REFERENCES

1. Olivier, Y.; Niedzialek, D.; Lemaur, V.; Pisula, W.; Müllen, K.; Koldemir, U.; Reynolds, J. R.; Lazzaroni, R.; Cornil, J.; Beljonne, D., 25th Anniversary Article: High-Mobility Hole and Electron Transport Conjugated Polymers: How Structure Defines Function. *Adv. Mater.* **2014**, *26*, 2119-2136.

2. Tsao, H. N.; Cho, D. M.; Park, I.; Hansen, M. R.; Mavrinskiy, A.; Yoon, D. Y.; Graf, R.; Pisula, W.; Spiess, H. W.; Müllen, K., Ultrahigh Mobility in Polymer Field-Effect Transistors by Design. *J. Am. Chem. Soc.* **2011**, *133*, 2605-2612.

3. Li, J.; Zhao, Y.; Tan, H. S.; Guo, Y.; Di, C.-A.; Yu, G.; Liu, Y.; Lin, M.; Lim, S. H.; Zhou, Y.; Su, H.; Ong, B. S., A Stable Solution-Processed Polymer Semiconductor with Record High-Mobility for Printed Transistors. *Sci. Rep.* **2012**, 2, 754.

4. Nketia-Yawson, B.; Lee, H.-S.; Seo, D.; Yoon, Y.; Park, W.-T.; Kwak, K.; Son, H. J.; Kim, B.; Noh, Y.-Y., A Highly Planar Fluorinated Benzothiadiazole-Based Conjugated Polymer for High-Performance Organic Thin-Film Transistors. *Adv. Mater.* **2015**, *27*, 3045-3052.

5. Venkateshvaran, D.; Nikolka, M.; Sadhanala, A.; Lemaur, V.; Zelazny, M.; Kepa, M.; Hurhangee, M.; Kronemeijer, A. J.; Pecunia, V.; Nasrallah, I.; Romanov, I.; Broch, K.; McCulloch, I.; Emin, D.; Olivier, Y.; Cornil, J.; Beljonne, D.; Sirringhaus, H., Approaching Disorder-Free Transport in High-Mobility Conjugated Polymers. *Nature* **2014**, *515*, 384-388.

6. Kim, G.; Kang, S.-J.; Dutta, G. K.; Han, Y.-K.; Shin, T. J.; Noh, Y.-Y.; Yang, C., A Thienoisoindigo-Naphthalene Polymer with Ultrahigh Mobility of 14.4 $cm^2V^{-1}s^{-1}$ That Substantially Exceeds Benchmark Values for Amorphous Silicon Semiconductors. *J. Am. Chem. Soc.* **2014**, *136*, 9477-9483.

7. Kang, I.; Yun, H.-J.; Chung, D. S.; Kwon, S.-K.; Kim, Y.-H., Record High Hole Mobility in Polymer Semiconductors *via* Side-Chain Engineering. *J. Am. Chem. Soc.* **2013**, *135*, 14896-14899.

8. Sun, B.; Hong, W.; Yan, Z.; Aziz, H.; Li, Y., Record High Electron Mobility of 6.3 $cm^2V^{-1}s^{-1}$ Achieved for Polymer Semiconductors Using a New Building Block. *Adv. Mater.* **2014**, *26*, 2636-2642.

9. Sirringhaus, H., 25th Anniversary Article: Organic Field-Effect Transistors: The Path Beyond Amorphous Silicon. *Adv. Mater.* **2014**, *26*, 1319-1335.

10. N. Taylor, P.; Huuskonen, J.; T. Aplin, R.; L. Anderson, H.; Huuskonen, J.; Rumbles, G.; Williams, E., Conjugated Porphyrin Oligomers from Monomer to Hexamer. *Chem. Commun.* **1998**, 909-910.

11. McCulloch, I.; Heeney, M.; Chabinyc, M. L.; DeLongchamp, D.; Kline, R. J.; Cölle, M.; Duffy, W.; Fischer, D.; Gundlach, D.; Hamadani, B.; Hamilton, R.; Richter, L.; Salleo, A.; Shkunov, M.; Sparrowe, D.; Tierney, S.; Zhang, W., Semiconducting Thienothiophene Copolymers: Design, Synthesis, Morphology, and Performance in Thin-Film Organic Transistors. *Adv. Mater.* **2009**, *21*, 1091-1109.

12. Mei, J.; Diao, Y.; Appleton, A. L.; Fang, L.; Bao, Z., Integrated Materials Design of Organic Semiconductors for Field-Effect Transistors. *J. Am. Chem. Soc.* **2013**, *135*, 6724-6746.

13. Tsao, H. N.; Müllen, K., Improving Polymer Transistor Performance *via* Morphology Control. *Chem. Soc. Rev.* **2010**, *39*, 2372-2386.

14. Noriega, R.; Rivnay, J.; Vandewal, K.; Koch, F. P. V.; Stingelin, N.; Smith, P.; Toney, M. F.; Salleo, A., A General Relationship between Disorder, Aggregation and Charge Transport in Conjugated Polymers. *Nat. Mater.* **2013**, *12*, 1038-1044.

15. Liscio, A.; Orgiu, E.; Mativetsky, J. M.; Palermo, V.; Samorì, P., Bottom-Up Fabricated Asymmetric Electrodes for Organic Electronics. *Adv. Mater.* **2010**, *22*, 5018-5023.

16. Koch, N., Organic Electronic Devices and Their Functional Interfaces. *ChemPhysChem* **2007**, *8*, 1438-1455.

17. Tsao, H. N.; Cho, D.; Andreasen, J. W.; Rouhanipour, A.; Breiby, D. W.; Pisula, W.; Müllen, K., The Influence of Morphology on High-Performance Polymer Field-Effect Transistors. *Adv. Mater.* **2009**, *21*, 209-212.

18. Sandberg, H. G. O.; Frey, G. L.; Shkunov, M. N.; Sirringhaus, H.; Friend, R. H.; Nielsen, M. M.; Kumpf, C., Ultrathin Regioregular Poly(3-hexyl thiophene) Field-Effect Transistors. *Langmuir* **2002**, *18*, 10176-10182.

19. Tang, C.; Tracz, A.; Kruk, M.; Zhang, R.; Smilgies, D.-M.; Matyjaszewski, K.; Kowalewski, T., Long-Range Ordered Thin Films of Block Copolymers Prepared by Zone-Casting and Their Thermal Conversion into Ordered Nanostructured Carbon. *J. Am. Chem. Soc.* **2005**, *127*, 6918-6919.

20. Tseng, H. R.; Phan, H.; Luo, C.; Wang, M.; Perez, L. A.; Patel, S. N.; Ying, L.; Kramer, E. J.; Nguyen, T. Q.; Bazan, G. C.; Heeger, A. J., High-Mobility Field-Effect Transistors Fabricated with Macroscopic Aligned Semiconducting Polymers. *Adv. Mater.* **2014**, *26*, 2993-2998.

21. Luo, C.; Kyaw, A. K. K.; Perez, L. A.; Patel, S.; Wang, M.; Grimm, B.; Bazan, G. C.; Kramer, E. J.; Heeger, A. J., General Strategy for Self-Assembly of Highly Oriented Nanocrystalline Semiconducting Polymers with High Mobility. *Nano Lett.* **2014**, *14*, 2764-2771.

22. Wang, G.; Persson, N.; Chu, P.-H.; Kleinhenz, N.; Fu, B.; Chang, M.; Deb, N.; Mao, Y.; Wang, H.; Grover, M. A.; Reichmanis, E., Microfluidic Crystal Engineering of π-Conjugated Polymers. *ACS Nano* **2015**, *9*, 8220-8230.

23. Bucella, S. G.; Luzio, A.; Gann, E.; Thomsen, L.; McNeill, C. R.; Pace, G.; Perinot, A.; Chen, Z.; Facchetti, A.; Caironi, M., Macroscopic and High-Throughput Printing of Aligned Nanostructured Polymer Semiconductors for MHz Large-Area Electronics. *Nat. Commun.* **2015**, 6, 8394.

24. Wang, S.; Kiersnowski, A.; Pisula, W.; Müllen, K., Microstructure Evolution and Device Performance in Solution-Processed Polymeric Field-Effect Transistors: The Key Role of the First Monolayer. *J. Am. Chem. Soc.* **2012**, *134*, 4015-4018.

25. Li, M.; Marszalek, T.; Zheng, Y.; Lieberwirth, I.; Müllen, K.; Pisula, W., Modulation of Domain Size in Polycrystalline n-Type Dicyanoperylene Mono- and Bilayer Transistors. *ACS Nano* **2016**, *10*, 4268-4273.

26. DiBenedetto, S. A.; Facchetti, A.; Ratner, M. A.; Marks, T. J., Molecular Self-Assembled Monolayers and Multilayers for Organic and Unconventional Inorganic Thin-Film Transistor Applications. *Adv. Mater.* **2009**, *21*, 1407-1433.

27. Hulea, I. N.; Fratini, S.; Xie, H.; Mulder, C. L.; Iossad, N. N.; Rastelli, G.; Ciuchi, S.; Morpurgo, A. F., Tunable Frohlich Polarons in Organic Single-Crystal Transistors. *Nat. Mater.* **2006**, *5*, 982-986.

28. Veres, J.; Ogier, S. D.; Leeming, S. W.; Cupertino, D. C.; Mohialdin Khaffaf, S., Low-k Insulators as the Choice of Dielectrics in Organic Field-Effect Transistors. *Adv. Funct. Mater.* **2003**, *13*, 199-204.

29. Stassen, A. F.; de Boer, R. W. I.; Iosad, N. N.; Morpurgo, A. F., Influence of the Gate Dielectric on the Mobility of Rubrene Single-Crystal Field-Effect Transistors. *Appl. Phys. Lett.* **2004**, *85*, 3899-3901.

30. Merari Masillamani, A.; Orgiu, E.; Samorì, P., Effect of the Molecular Weight of the Polymer Gate Dielectric on the Performances of Solution-Processed Ambipolar OTFTs. *J. Mater. Chem. C* **2013**, *1*, 7725-7730.

31. Gaikwad, A. M.; Khan, Y.; Ostfeld, A. E.; Pandya, S.; Abraham, S.; Arias, A. C., Identifying Orthogonal Solvents for Solution Processed Organic Transistors. *Org. Electron.* **2016**, *30*, 18-29.

32. Ariga, K.; Yamauchi, Y.; Mori, T.; Hill, J. P., 25th Anniversary Article: What Can Be Done with the Langmuir-Blodgett Method Recent Developments and its Critical Role in Materials Science. *Adv. Mater.* **2013**, *25*, 6477-6512.

33. Musumeci, C.; Salzmann, I.; Bonacchi, S.; Röthel, C.; Duhm, S.; Koch, N.; Samorì, P., The Relationship between Structural and Electrical Characteristics in Perylenecarboxydiimide-Based Nanoarchitectures. *Adv. Funct. Mater.* **2015**, *25*, 2501-2510.

34. Fabiano, S.; Musumeci, C.; Chen, Z.; Scandurra, A.; Wang, H.; Loo, Y.-L.; Facchetti, A.; Pignataro, B., From Monolayer to Multilayer N-Channel Polymeric Field-Effect Transistors with Precise Conformational Order. *Adv. Mater.* **2012**, *24*, 951-956.

35. Xu, G.; Bao, Z.; Groves, J. T., Langmuir–Blodgett Films of Regioregular Poly(3-hexylthiophene) as Field-Effect Transistors. *Langmuir* **2000**, *16*, 1834-1841.

36. Natali, D.; Sampietro, M.; Franco, L.; Bolognesi, A.; Botta, C., Mobility Anisotropy in Langmuir–Blodgett Deposited Poly(3-Methoxypentyl-Tiophene)-Based Thin Film Transistors. *Thin Solid Films* **2005**, *472*, 238-241.

37. D'Innocenzo, V.; Luzio, A.; Abdalla, H.; Fabiano, S.; Loi, M. A.; Natali, D.; Petrozza, A.; Kemerink, M.; Caironi, M., Two-Dimensional Charge Transport in Molecularly Ordered Polymer Field-Effect Transistors. *J. Mater. Chem. C* **2016**, *4*, 11135-11142.

38. Lei, T.; Cao, Y.; Fan, Y.; Liu, C.-J.; Yuan, S.-C.; Pei, J., High-Performance Air-Stable Organic Field-Effect Transistors: Isoindigo-Based Conjugated Polymers. *J. Am. Chem. Soc.* **2011**, *133*, 6099-6101.

39. Lei, T.; Wang, J.-Y.; Pei, J., Design, Synthesis, and Structure–Property Relationships of Isoindigo-Based Conjugated Polymers. *Acc. Chem. Res.* **2014**, *47*, 1117-1126.

40. Lei, T.; Dou, J.-H.; Pei, J., Influence of Alkyl Chain Branching Positions on the Hole Mobilities of Polymer Thin-Film Transistors. *Adv. Mater.* **2012**, *24*, 6457-6461.

41. Tseng, H. R.; Ying, L.; Hsu, B. B. Y.; Perez, L. A.; Takacs, C. J.; Bazan, G. C.; Heeger, A. J., High Mobility Field Effect Transistors Based on Macroscopically Oriented Regioregular Copolymers. *Nano Lett.* **2012**, *12*, 6353-6357.

42. Sirringhaus, H.; Wilson, R. J.; Friend, R. H.; Inbasekaran, M.; Wu, W.; Woo, E. P.; Grell, M.; Bradley, D. D. C., Mobility Enhancement in Conjugated Polymer Field-Effect Transistors Through Chain Alignment in a Liquid-Crystalline Phase. *Appl. Phys. Lett.* **2000**, *77*, 406-408.

43. Zhokhavets, U.; Gobsch, G.; Hoppe, H.; Sariciftci, N. S., A Systematic Study of the Snisotropic Optical Properties of Thin Poly(3-Octylthiophene)-Films in Dependence on Growth Parameters. *Thin Solid Films* **2004**, *451–452*, 69-73.

44. Lee, M. J.; Gupta, D.; Zhao, N.; Heeney, M.; McCulloch, I.; Sirringhaus, H., Anisotropy of Charge Transport in a Uniaxially Aligned and Chain-Extended, High-Mobility, Conjugated Polymer Semiconductor. *Adv. Funct. Mater.* **2011**, *21*, 932-940.

45. Cativo, M. H. M.; Kim, D. K.; Riggleman, R. A.; Yager, K. G.; Nonnenmann, S. S.; Chao, H.; Bonnell, D. A.; Black, C. T.; Kagan, C. R.; Park, S.-J., Air–Liquid Interfacial Self-Assembly of Conjugated Block Copolymers into Ordered Nanowire Arrays. *ACS Nano* **2014**, *8*, 12755-12762.

46. Minder, N. A.; Ono, S.; Chen, Z.; Facchetti, A.; Morpurgo, A. F., Band-Like Electron Transport in Organic Transistors and Implication of the Molecular Structure for Performance Optimization. *Adv. Mater.* **2012**, *24*, 503-508.